Multi-body Optimization with Subject-Specific Knee Models: Performance at High Knee Flexion Angles

Caecilia Charbonnier[1]*, Sylvain Chagué[1], Frank C. Kolo[2], Victoria B. Duthon[3], Jacques Ménétrey[3]

[1] *Medical Research Department, Artanim Foundation, Geneva, Switzerland*

[2] *Rive Droite Radiology Center, Geneva, Switzerland*

[3] *Centre de Médecine de l'appareil locomoteur et du sport, Orthopedics and Trauma Service, University Hospitals of Geneva, Geneva, Switzerland*

Corresponding author:

Caecilia Charbonnier, PhD

Artanim Foundation

40, chemin du Grand-Puits – 1217 Meyrin, Switzerland

Telephone number: +41 22 980 91 92

E-mail address: caecilia.charbonnier@artanim.ch

None of the authors have any conflicts of interest to disclose.

Multi-body Optimization with Subject-Specific Knee Models: Performance at High Knee Flexion Angles

When estimating knee kinematics from skin markers and stereophotogrammetry, multi-body optimization (MBO) has provided promising results for reducing soft tissue artefacts (STA), but can still be improved. The goal of this study was to assess the performance of MBO with subject-specific knee models at high knee flexion angles (up to 110°) against knee joint kinematics measured by magnetic resonance imaging. Eight subjects were recruited. MBO with subject-specific knee models was more effective in compensating STA compared to no kinematic and spherical constraints, in particular for joint displacements. Moreover, it seems to be more reliable over large ranges of knee flexion angle. The ranges of root mean square errors for knee rotations / displacements were 3.0°-9.2° / 1.3-3.5 mm for subject-specific knee models, 6.8°-8.7° / 6.0-12.4 mm without kinematic constraint and 7.1°-9.8° / 4.9-12.5 mm for spherical constraints.

Keywords: Soft tissue artefact; Knee; Multi-body optimization, Joints and ligament constraints, Subject-specific modeling; High knee flexion

Introduction

Stereophotogrammetry and the use of skin markers are a widely recognized technique to analyze human movement. The aim is to deduce the kinematics of the bone segments under investigation from the trajectories of the skin markers. However, such technique is subject to soft tissue artifacts (STA) due to muscle contractions and skin sliding, causing the markers to move with respect to the underlying bone (Leardini et al.2005). In the lower extremity, the thigh is particularly affected. To solve this issue, several techniques were proposed. Some of them computed the optimal bone pose from a marker cluster by considering each segment separately (Söderkvist and Wedin1993; Chèze et al.1995), while other methods, such as multi-body optimization (MBO) (Lu and O'Connor1999; Duprey et al.2010; Bergamini et al.2011; Gasparutto et al.2015; Clément et al.2015; Richard et al.2016; Clément et al.2017; Richard et al.2017), aimed

at optimally estimating the location of bone segments, modelled as a kinematic chain of rigid bodies connected by articulating joints, by minimizing the distances between the model-determined and the measured marker trajectories. A recent review on the use and applications of MBO is given in Leardini et al. (2017).

The use of MBO for determining knee kinematics provided promising results (Duprey et al.2010; Gasparutto et al.2015; Clément et al.2015; Richard et al.2016), but validation of the method remains limited. In particular, MBO methods rely on the determination of a predefined kinematic model with specific joint constraints. Simple kinematic constraints (spherical or hinge joints) were introduced, but showed mixed results. Stagni et al. (2009), Andersen et al. (2010), Clément et al. (2017) and Richard et al. (2017) obtained significant errors at the knee level evidencing limitations in reducing STA, especially its effect on joint translations. Opposite results were found in Gasparutto et al. (2015) and Richard et al. (2016) where spherical constraints performed better than models with no kinematic constraint, leading the authors to conclude that imposing joint constraints could be valuable. These studies suggested that more advanced models implementing anatomical constraints, together with accurate parameter identification, could improve results.

Anatomical constraints were thus proposed by taking into account the articular surfaces and the ligaments. Duprey et al. (2010) and Clément et al. (2017) modeled the knee using parallel mechanisms with sphere-on-plane contacts (Feikes et al.2003) and three isometric ligaments of constant length: anterior cruciate ligament (ACL), posterior cruciate ligament (PCL) and medial collateral ligament (MCL). This concept was further developed in Bergamini et al. (2011), Gasparutto et al. (2013) and Gasparutto et al. (2015) taking into account the four major ligaments (ACL, PCL, MCL and the lateral medial collateral ligament (LCL)) and different deformable conditions: minimal

ligament length variations or prescribed ligament length variations as a function of knee flexion angle. The latter study concluded that anatomical constraints helped reduce STA compared to no kinematic constraint or degree-of-freedom (DoF) coupling curves (Walker et al.1988). To account for ligament deformability, a “soft” constraint (i.e., stiffness matrix) and a penalty-based method were also introduced in Richard et al. (2016). The authors suggested as in Gasparutto et al. (2015) that for a better definition of joint models, personalization should be considered for further improvements.

The importance of improving the accuracy of kinematic models to reduce the errors in calculated joint kinematics using personalization from medical imaging has been demonstrated previously (Scheys et al.2011; Clément et al.2015; Valente et al.2015; Sreenivasa et al.2016; Kainz et al.2016). In particular, Clément et al. (2015) evaluated the performance of knee joint models with subject-specific kinematic constraints in healthy and osteoarthritis subjects during quasi-static squats. Different kinematic chains of four lower limb segments were compared using various combinations of joint models (a mix of no kinematic constraint, spherical joints and parallel mechanisms with customized minimal ligaments length variation). Results showed that personalization improved STA compensation, especially for the knee internal/external rotation, abduction/adduction, antero-posterior and proximal-distal displacements in both groups of tested subjects. This is to our knowledge the only work to date assessing personalized knee models in MBO for STA compensation. Therefore, further investigation is required to attest their validity.

Another aspect common to all previously cited studies is that the knee ranges of motion (ROM) of the activities considered in the in vivo experiments were limited to small flexion angles (usually between 40-65°). Indeed, these studies focused on typical clinical movements (e.g. gait, running, limited squat), but for many sport activities (e.g.

dance, gymnastic, judo, hockey) higher ROM is usually performed. The performance of MBO at higher knee flexion angles should be hence verified and we expected that the more advanced models such as parallel mechanism would provide better results, since they are able to more realistically model the complex physiological kinematic behavior of the knee that comes into play at higher ROM (i.e., knee rollback) (Duprey et al.2010; Leardini et al.2017).

The objective of this study was thus to assess against in vivo knee joint kinematics measured by Magnetic Resonance Imaging (MRI) the performance of MBO with subject-specific knee models. Here, we introduced more refined knee joint models to reproduce, at best, specific knee geometry: the standard sphere-on-plane contacts were replaced by surface-on-plane contacts, and the ligaments attachment sites were defined with reference to MRI. Moreover, the performance of MBO is evaluated at high knee flexion angles, up to 110°. For comparison, MBO methods with no kinematic and with spherical constraints were also studied.

Materials and methods

Subjects

The measurements were made on the right knee of eight healthy young active participants (five females, three males). The mean age, weight and height were 27.1 years, 61.3 kg and 166 cm, respectively. Because of the technical protocol, a height criterion was used. The subjects higher than 180 cm were excluded. Other exclusion criteria were reported previous knee injuries, knee surgery or contraindications for MRI. Institutional ethical approval and informed consent were obtained prior to data collection.

Experimental protocol

All volunteers were MRI scanned with a 1.5 T Optima MR450w GEM system (General Electric Healthcare, Milwaukee, WI, USA). A flexible surface coil was used and images were acquired at several unloaded knee flexions: 0°, 45°, 90° and 110°. At neutral knee flexion (0°), the subjects were placed in supine position. One 3D intermediate weighted fast spin echo without fat saturation (Cube®) sequence (section thickness 0.8 mm; no gaps; TR/TE ms 1500/27.9) centered on the knee and three 3D fast gradient echo (Lava®) sequences (section thickness 3 mm; no gaps; TR/TE ms 4.2/2.0) were achieved covering a region of interest from the pelvis to the ankle, as shown in Figure 1A. For the other flexion angles, the subjects were lying on the right side to ensure sufficient room to center the knee joint in the magnetic bore. A hand-held goniometer was used to position the subject's lower limb at the desired knee flexion. For each position, one 3D intermediate weighted fast spin echo without fat saturation (Cube®) sequence and two 3D fast gradient echo (Lava®) sequences were acquired (Figure 1B). It is worth mentioning that changing orientation of the body in the MRI scanner resulted in soft tissues shape changes.

The subjects were equipped with external MRI-compatible markers set placed directly onto the skin using adhesive tape. We used spherical capsules (Ø10 mm) of Burgenstein Vitamin E (Antistress AG, Switzerland) because of their highly visible MRI signal. The femur marker set included three markers placed on anatomical landmarks (greater trochanter, lateral and medial femoral epicondyles) and four markers distributed on the lateral and frontal parts of the thigh (see Figure 1). For the tibia, three markers were placed on anatomical landmarks (tibial tuberosity, medial and lateral malleoli), one on the lateral part and one on the medial part of the shank. Markers were placed as much as possible on skin areas susceptible to show less sensitivity to STA

according to previous studies (Stagni et al.2005; Akbarshahi et al.2010; Kuo et al.2011; Tsai et al.2011). The same investigator (CC) attached all markers and performed all measurements.

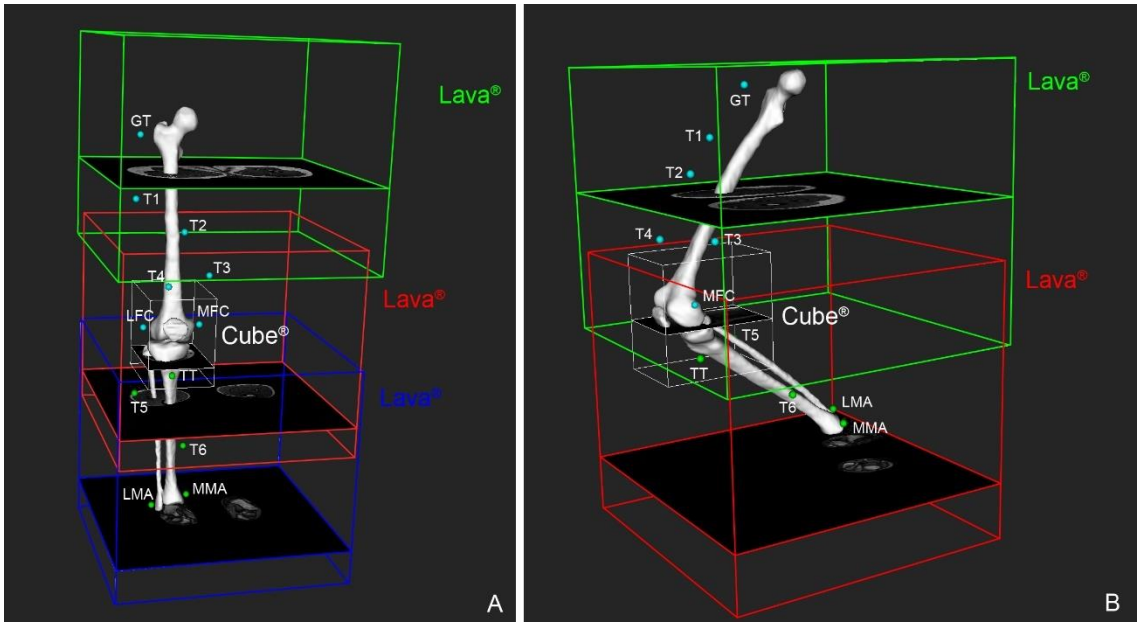

Figure 1. MRI volumes acquired A) in neutral knee flexion (frontal view) and B) at 90° knee flexion (lateral view). Markers are also shown. GT = greater trochanter, LFC = lateral femoral epicondyle, MFC = medial femoral epicondyle, TT = tibial tuberosity, MMA = medial malleoli, LMA = lateral malleoli, T1-T6 = technical markers.

Kinematic knee models

Bone geometry was obtained from 3D reconstruction based on the 3D images in neutral knee flexion. The MRI volumes were registered and manually segmented using Mimics software (Materialize NV, Leuven, Belgium). For each volunteer, subject-specific 3D models of the femur and tibia were thus obtained.

Parallel mechanism was modeled with four ligaments (ACL, PCL, MCL, LCL) and two surface-on-plane contacts, providing more accurate constraints than the standard sphere-on-plane contacts, since it takes into account the femur geometry and not an approximation. The surface-on-plane constraints forced the lateral and medial femoral condyles surfaces to maintain contact with the tibial plateaus, modeled as a 3D

plane. The contact surfaces and the normal and point of planes were determined on the subject-specific knee bone models. To account for the articular cartilages, the tibial plateaus plane was then translated superiorly along its normal by the average thickness of the cartilages. We estimated this value to 4 mm (2 mm for the femoral and tibial cartilages, respectively) based on literature measuring cartilage thickness at the joint (Cohen et al.1999; Shepherd and Seedhom1999).

The origins and insertions of the four ligaments were defined for each subject by first identifying on the high-resolution 3D Cube® images the attachment surface and then taking its barycenter. Ligament length variations measured in all subjects during the experiment were fitted with polynomial functions of the knee flexion angle θ. Table 1 provides for each ligament the computed coefficients of the polynomial interpolation. A leave-one-out analysis was performed for each ligament to evaluate how well the polynomial interpolation would generalize to an independent dataset. The computed leave-one-out cross validation errors are given in Table 1, showing that the ligament length variation models were not overfitting the data.

Table 1. Coefficients of the polynomial interpolation* used to fit ligament length variations (% of elongation compared to the length at neutral knee flexion) with respect to the knee flexion angle θ. The last column provides the leave-one-out cross validation error (LOO-XVE) for each ligament evaluating how well the polynomial interpolation would generalize to an independent dataset.

	ACL (l = 1)	PCL (l = 2)	MCL (l = 3)	LCL (l = 4)
α_0^l	0.9963	0.9996	0.9974	1.0037
α_1^l	0.0012	-0.0045	-0.0004	-0.0003
α_2^l	1.58e-05	-2.54e-05	-1.23e-05	-1.09e-05
LOO-XVE	0.052	0.060	0.042	0.046

* $d^l(\theta) = a_0^l + a_1^l\theta + a_2^l\theta^2$

Multi-body optimization and constraints

The aim of MBO is to minimize the sum of square distances between model-determined and measured skin marker positions by optionally taking into account a certain number of kinematic constraints (Lu and O'Connor1999; Duprey et al.2010; Gasparutto et al.2015; Richard et al.2016; Clément et al.2017; Richard et al.2017). In this study, MBO was applied to two segments – the femur and the tibia. Three different kinematic models were considered: First, no kinematic constraint (N) was imposed to the knee joint (full 6 DoF), equivalent to a least square segment pose estimation, such as the singular value decomposition (SVD) (Söderkvist and Wedin1993). Second, a spherical joint constraint (S) (Lu and O'Connor1999) was introduced limiting movement to rotation only (3 DoF). The center of rotation was taken as the midpoint between the lateral and medial femoral epicondyles. Third, parallel mechanism constraints (P) were applied considering the two surface-on-plane contacts and the four ligament length variations, implemented as a penalty-based method (Gasparutto et al.2013; Charbonnier et al.2014) as follows:

$$min \sum_{s=1}^{2} \left(\sum_{i=1}^{n_s} \alpha_{si} \| T_s x_{si} - y_{si} \|^2 \right) + \beta \sum_{e=1}^{2} D_e^2 + \sum_{l=1}^{4} \gamma_l (L_l - Lref_l)^2 \quad (1)$$

The optimal pose T_s (i.e., 3 rotational components (r_x, r_y, r_z) and 3 translational components (t_x, t_y, t_z)) for each segment s corresponds to the minimization of three terms:

- the square distances between the model-based (x_{si}) and the measured (y_{si}) marker coordinates in the segment's cluster (n_s markers in segment's cluster s) with a weighting factor α_{si} to reflect different degrees of STA, as described by Lu and O'Connor (1999);

- the square distance D_e^2 between the lateral ($e = 1$) or medial ($e = 2$) condyle surface and the tibial plateaus plane translated superiorly along its normal by 4 mm for the given pose with a weighting factor β, where D_e is the minimum of the distances between each point of the condyle and the tibial plateaus plane (note that under the modelling assumption that cartilage thickness is constant over the whole articular surfaces and between subjects, this term tends to zero);
- the square difference between the computed ligament length L_l for the ligament l and the reference ligament length $Lref_l$ obtained by multiplying the rest length (measured at neutral knee flexion) with the estimated variation calculated for the given pose with the polynomial interpolation (see Table 1) and weighted by γ_l to reflect different ligament contributions. Given the large ROM studied, prescribed ligament length variations were preferred over minimized ligament length variations around the average length.

The model-based (x_{si}) marker coordinates were established in neutral knee flexion. For all kinematic models and for simplicity, equal weighting factors ($\alpha_{si} = \frac{1}{n_s}$) were assigned to the markers of the femur and tibia. No different weighting factor was applied between the surface-on-plane constraints ($\beta = \frac{1}{2}$), nor between the ligaments ($\gamma_l = \frac{1}{4}$). Overall, the distribution of weights between the three terms of Equation (1), which are all homogeneous to a squared distance, was chosen so that each term was of the same order of magnitude. The initial guess used in MBO was computed from the skin markers using SVD. Equation (1) was solved by a non-linear BFGS optimization (Byrd et al.1995).

Validation procedure

In order to assess the performance of the three models used in MBO to compensate for STA at several knee flexions, model-based knee kinematics derived from the skin markers was compared to the knee kinematics derived from the MRI scans. The MR series were processed, the bones segmented and the reference bone positions and orientations were calculated by registering the subject-specific knee bone models to each MRI pose using the iterative closest point algorithm (Besl and McKay1992). Skin markers visible on the MR images were manually labelled and the centers of gravity of each marker were determined.

After MBO, descriptive statistics and in particular the root mean square errors (RMSEs) between the model-based and the reference kinematics were computed for each method at each flexion angle and for the overall ROM (i.e., cumulated data for the three flexion angles). Knee joint angles and displacements were calculated with the femur and tibia segment coordinate systems defined following the recommendations of the ISB (Wu et al.2002) using anatomical landmarks identified on the subject-specific knee bone models by virtual palpation. The center of the femoral head was calculated using a sphere fitting method (Schneider and Eberly2003).

Results

RMSEs between the model-based knee kinematics computed by the three MBO methods and the reference kinematics at 45°, 90° and 110° of knee flexion and for the entire ROM are shown in Figure 2. Figure 3 presents box-and-whisker plots of the kinematic errors. Information about the actual ROM at the different knee flexion angles is also reported in Table 2.

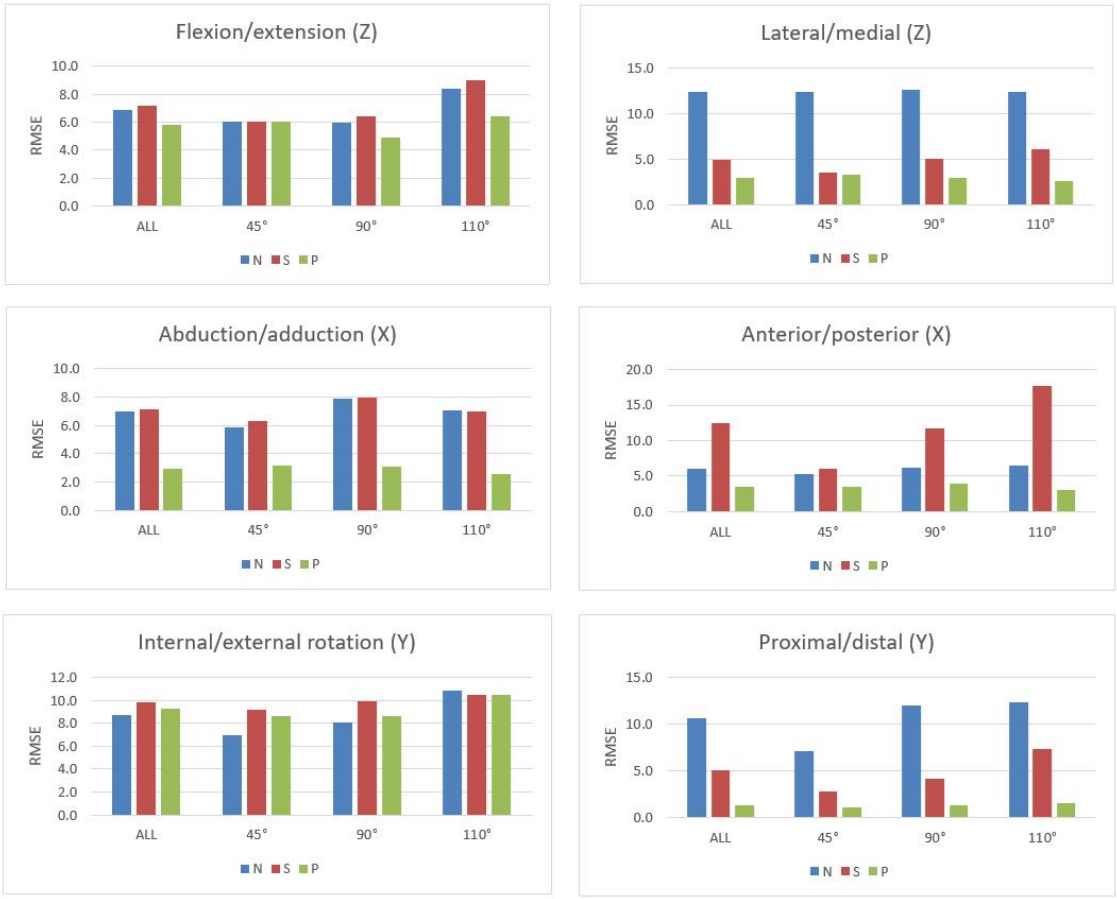

Figure 2. RMSEs for the three MBO methods at various knee flexion angles (45°, 90° and 110°) and for the overall ROM.

Table 2. Mean ± standard deviation of the actual ROM at 45°, 90° and 110° of knee flexion. Abduction (-) / adduction (+), AA; internal (+) / external (-) rotation, IE; lateral (+) / medial (-) displacement, LM; anterior (+) / posterior (-) displacement, AP; and proximal (+) / distal (-) displacement, PD.

Flexion angle	AA (°)	IE (°)	LM (mm)	AP (mm)	PD (mm)
45°	7.8 ± 4.0	1.0 ± 7.8	-3.1 ± 1.3	6.4 ± 3.6	0.0 ± 3.5
90°	6.4 ± 4.4	7.2 ± 6.2	-4.6 ± 1.4	12.1 ± 2.6	1.7 ± 5.4
110°	4.9 ± 3.2	9.1 ± 6.2	-6.0 ± 1.8	17.4 ± 1.7	3.6 ± 6.5

Overall, the lowest RMSEs in all anatomical planes were obtained with the parallel mechanism constraints. Compared to constraints N and S, the model P was particularly good in minimizing displacements errors (between 1.3 and 3.5 mm vs. 6.0 and 12.4 mm and 4.9 and 12.5 mm for N and S, respectively). RMSEs for flexion/extension and abduction/adduction obtained with model P were also smaller (5.8° and 3.0°, respectively), but were comparable for internal/external rotation compared to the other models (9.2°). For constraints N and S, the RMSEs among the joint angles showed comparable results (difference of 1°), while the model S was more accurate than the model N for lateral-medial and proximal-distal displacements, but less accurate for the anterior-posterior shift.

In terms of inter-subject variability, model P demonstrated globally the best median and inter-quartile of errors (Figure 3), in particular for abduction/adduction and proximal-distal displacements. For all flexion angles, constraints N and S exhibited comparable variability across subjects, but model S depicted smaller inter-quartile ranges than model N for displacement errors.

RMSEs for flexion/extension increased for constraints N and S with higher knee flexion angles, whereas RMSEs were in the similar range over all flexion angles for model P. For the other anatomical planes, as well as for displacements, parallel mechanism constraints seem to have more stable errors across the whole ROM. Interestingly, RMSEs for internal/external rotation were high for the three methods.

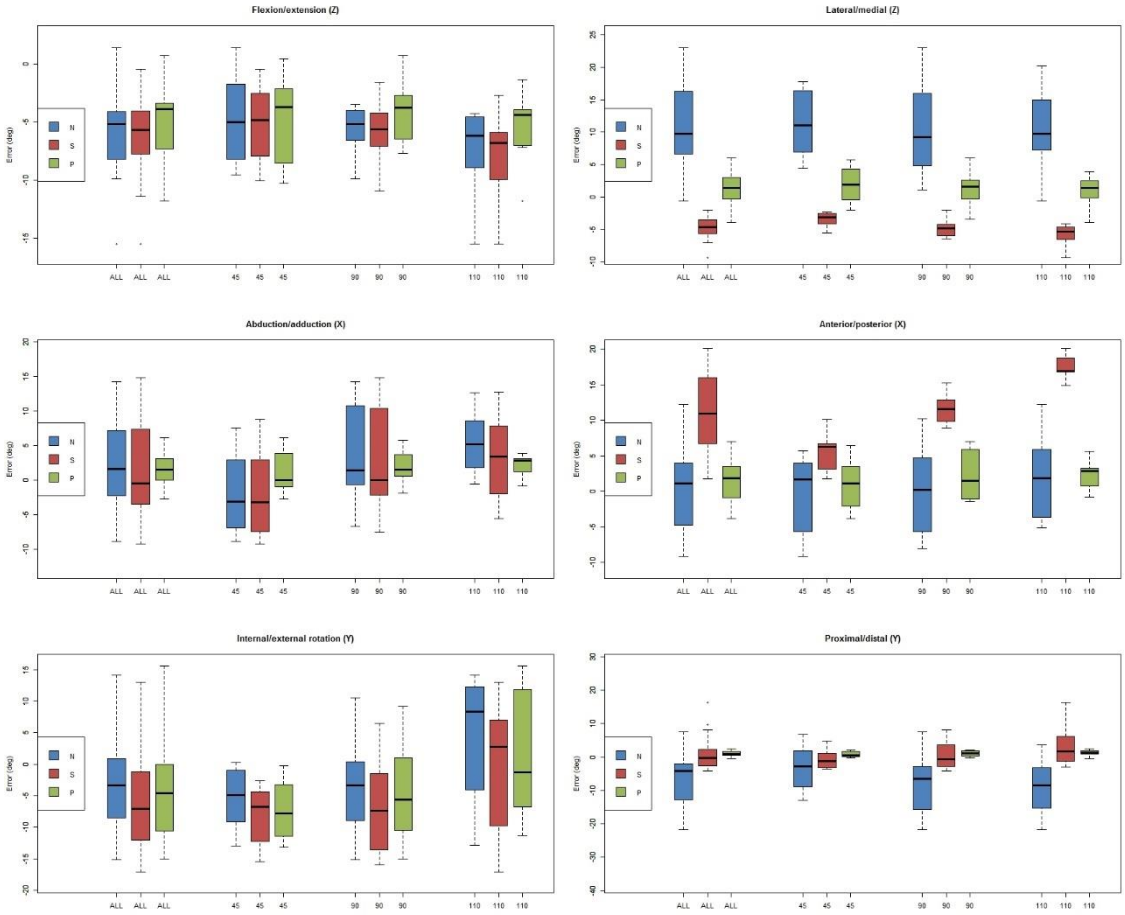

Figure 3. Box-and-whisker plots of the kinematic errors for the three MBO methods at various knee flexion angles (45°, 90° and 110°) and for the overall ROM.

Discussion

In this study, we compared three MBO methods with different joint constraints against in vivo knee joint kinematics measured by MRI at high knee flexion angles. Moreover, we introduced anatomical constraints based on subject-specific knee joint models, taking into account personalized ligaments attachment sites and knee bone geometry. This is the first in vivo study evaluating the performance of MBO methods at high knee flexion angles, up to 110°.

Defining a kinematic model to be used in MBO in order to derive accurate knee joint kinematics based on skin markers is critical. The use of no kinematic constraint or spherical constraints was thoroughly analyzed (Stagni et al.2009; Andersen et al.2010;

Gasparutto et al.2015; Richard et al.2016; Clément et al.2017; Richard et al.2017) showing mixed results but most often inaccurate model-based kinematics. For instance, Stagni et al. (2009) reported mean RMSEs between 8° and 13° for knee rotations and between 5 and 20 mm for knee displacements during squatting. In the same activity, Clément et al. (2017) recorded mean RMSEs around 3-8° for knee rotations but less errors for knee displacements (2-3 mm). Our results for the spherical model were similar showing large RMSEs for all anatomical planes and in particular for joint displacements. According to our findings, the use of parallel mechanisms with subject-specific knee models gave lower error ranges, except for internal/external rotation. Indeed, RMSEs for internal/external rotation were not improved but comparable with the methods with no kinematic or with spherical constraints and were also high. Whereas the two latter models impose no limitation in rotational movement, parallel mechanisms attempt to reproduce the biomechanical behavior of the knee ligaments that play a role in stabilizing the joint and thus limiting excessive ROM, which did not improve results for internal/external rotation in the present study. One explanation could be that the subjects were lying on the side during the MRI acquisitions. Abnormal STA were likely to be induced by soft tissue compression of the leg in contact with the MRI table, as well as by the change of gravity compared to the MRI acquisitions in supine position for the neutral knee flexion.

For quasi-static squats studied at five knee positions (0°, 30°, 40°, 50° and 60°), Clément et al. (2015) compared model-based kinematics measured using the KneeKG™ – a motion capture device designed to limit STA (Lustig et al.2012) – with the kinematics measured by biplanar radiographic imaging system (EOS®) on 10 subjects. Using subject-specific kinematic constraints, they reported RMSEs of 2.2 ± 1.2° and 5.2 ± 3.8° for abduction/adduction and internal/external rotation, respectively, and 4.3 ± 2.4

mm, 3.2 ± 2.1 mm and 2.4 ± 1.1 mm for medial/lateral, anterior/posterior and proximal/distal displacements, respectively. The use of the subject-specific kinematic constraints in the present study gave better accuracy for joint displacements, but greater errors for joint angles. These greater errors could be explained by the fact that the KneeKG™ device tackled STA more effectively than the marker set used in the present study. Moreover, we investigated larger ROM up to 110°, thus more important STA could be expected. Finally, Clément et al. (2015) used a complete lower limb model (4 segments and 3 joints, from the hip to the foot) in MBO, resulting in better optimization performances as previously reported (Duprey et al.2010).

Another foreseen finding of the present study is that the parallel mechanism constraints seem to have more stable errors across the whole ROM and less inter-subject variability. Compared to simple kinematic constraints, errors did not increase with knee flexion angle, and the results of model P demonstrated the best median and inter-quartile of errors. Indeed, these mechanisms seemed to model appropriate physiological knee patterns (i.e. femoral rollback, limited abduction/adduction), as previously evidenced (Duprey et al.2010; Leardini et al.2017). Furthermore, they have the unique advantage of being customizable with subject-specific knee joint geometry, hence offering the possibility to adapt the model to pathologies and to conduct clinical studies. STA being known to be subject-specific (Leardini et al.2005), adding more personalized anatomical constraints is also expected to reduce more effectively the inter-subject variability of the model-derived kinematics.

We acknowledge some limitations in the present study. First, we assessed the performance of MBO methods in reducing STA errors against in vivo knee joint kinematics measured by MRI during static and non-weight-bearing knee poses, which does not represent dynamic activities for which STA would be different (due to inertia

effects, muscle contractions, etc.). In the literature, two types of technique are generally used as gold standard to evaluate methods for STA compensation. The first type uses strongly invasive metallic rods inserted directly into the bone and instrumented with cluster of markers to derive true bone movements, such as intra-cortical pins (Benoit et al.2006; Gasparutto et al.2015; Richard et al.2017). The second type uses fluoroscopic acquisitions (Stagni et al.2005; Lin et al.2016; Richard et al.2016; Richard et al.2017) which has two main drawbacks: firstly, the 3D movement is estimated from biplanar radiographs and secondly the method uses ionizing radiation. Conversely, MRI acquisitions are not invasive and provides full 3D images of the joint with visualization of the soft tissues, but the volumes of the knee need to be acquired in static positions. Therefore, we consider this technique more suitable for a study involving healthy volunteers. Another limitation was that the parallel mechanisms used in MBO to compute model-based knee kinematics of the subjects were based on polynomial functions built from the validation data obtained from the same subjects, which represents a source of bias. Eventually, instead of using a constant cartilage thickness in the sphere-on-plane constraints, cartilages could have been segmented on MRI to obtain subject-specific and accurate thickness estimation of these structures, but this would have required an invasive arthro-MRI (with injection of contrast agent) to allow for a reliable segmentation of the soft tissues.

Conclusion

The results of this study seem to confirm the findings of Clément et al. (2015) and indicate that MBO combined with subject-specific knee models can improve knee kinematics estimation based on skin markers, in particular for the determination of joint displacements. In addition, this method seems to be more reliable over large ranges of knee flexion angle, since it models more precisely the physiological behavior of the

knee joint. Although this method should be further validated with large ROM during dynamic movements, it provides promising results for the study of pathologies or injuries related to sport activities requiring high knee flexion.

References:

Akbarshahi, M., Schache, A., Fernandez, J., Baker, R., Banks, S., and Pandy, M. (2010). Non-invasive assessment of soft-tissue artifact and its effect on knee joint kinematics during functional activity. *J Biomech*, 43:1292–1301.

Andersen, M., Benoit, D., Damsgaard, M., Ramsey, D., and Rasmussen, J. (2010). Do kinematic models reduce the effects of soft tissue artefacts in skin marker-based motion analysis? An in vivo study of knee kinematics. *J Biomech*, 43:268–273.

Benoit, D., Ramsey, D., Lamontagne, M., Xu, L., P., P. W., and Renstroem (2006). Effect of skin movement artifact on knee kinematics during gait and cutting motions measured in vivo. *Gait & Posture*, 24(2):152–164.

Bergamini, E., Pillet, H., Hausselle, J., Thoreux, P., Guerard, S., Camomilla, V., Cappozzo, A., and Skalli, W. (2011). Tibio-femoral joint constraints for bone pose estimation during movement using multi-body optimization. *Gait & Posture*, 33(4):706–711.

Besl, P. and McKay, N. (1992). A method for registration of 3-D shapes. *IEEE Transactions on Pattern Analysis and Machine Intelligence*, 14(2):239–256.

Byrd, R., Lu, P., Nocedal, J., and Zhu, C. (1995). A limited memory algorithm for bound constrained optimization. *SIAM J Scientific Comput*, 16(5):1190–1208.

Charbonnier, C., Chagué, S., Kolo, F., Chow, J., and Lädermann, A. (2014). A patient-specific measurement technique to model the kinematics of the glenohumeral joint. *Orthop & Traumatol: Surg & Res*, In Press.

Chèze, L., Fregly, B., and Dimnet, J. (1995). A solidification procedure to facilitate kinematic analyses based on video system data. *J Biomech*, 28:879–884.

Clément, J., Dumas, R., Hagemeister, N., and de Guise, J. (2017). Can generic knee joint models improve the measurement of osteoarthritic knee kinematics during squatting activity? *Comput Meth Biomech Biomed Eng*, 20(1):94–103.

Clément, J., R. Dumas and, N. H., and de Guise, J. (2015). Soft tissue artifact compensation in knee kinematics by multi-body optimization: Performance of subject-specific knee joint models. *J Biomech*, 48:3796–3802.

Cohen, Z., McCarthy, D., Kwak, S., Legrand, P., Fogarasi, F., Ciaccio, E., and Ateshian, G. (1999). Knee cartilage topography, thickness, and contact areas from MRI: In- vitro calibration and in-vivo measurements. *Osteoarthritis and Cartilage*, 7(1):95–109.

Duprey, S., Chèze, L., and Dumas, R. (2010). Influence of joint constraints on lower limb kinematics estimation from skin markers using global optimization. *J Biomech*, 43(14):2858–2862.

Feikes, J., O'Connor, J., and Zavatsky, A. (2003). A constraint-based approach to modelling the mobility of the human knee joint. *J Biomech*, 36(1):125–129.

Gasparutto, X., Dumas, R., and Jacquelin, E. (2013). Multi-body optimisation with deformable ligament constraints: influence of ligament geometry. *Comput Meth Biomech Biomed Eng*, 15:191–193.

Gasparutto, X., Sancisi, N., Jacquelin, E., Parenti-Castelli, V., and Dumas, R. (2015). Validation of a multi-body optimization with knee kinematic models including ligament constraints. *J Biomech*, 48:1141–1446.

Kainz, H., Modenese, L., Lloyd, D., Maine, S., Walsh, H., and Carty, C. (2016). Joint kinematic calculation based on clinical direct kinematic versus inverse kinematic gait models. *J Biomech*, 49(9):1658–1669.

Kuo, M.-Y., Tsai, T.-Y., Lin, C.-C., Lu, T.-W., Hsu, H.-C., and Shen, W.-C. (2011). Influence of soft tissue artifacts on the calculated kinematics and kinetics of total knee replacements during sit-to-stand. *Gait & Posture*, 33(3):379–384.

Leardini, A., Belvedere, C., Nardini, F., Sancisi, N., Conconi, M., and Parenti-Castelli, V. (2017). Kinematic models of lower limb joints for musculo-skeletal modelling and optimization in gait analysis. *J Biomech*, 62:77-86.

Leardini, A., Chiari, L., Croce, U. D., and Cappozzo, A. (2005). Human movement analysis using stereophotogrammetry Part 3: Soft tissue artifact assessment and compensation. *Gait & Posture*, 21:212–225.

Lin, C.-C., Lu, T.-W., Lu, H.-L., Kuo, M.-Y., and Hsu, H.-C. (2016). Effects of soft tissue artifacts on differentiating kinematic differences between natural and replaced knee joints during functional activity. *Gait & Posture*, 46:154–160.

Lu, T. and O'Connor, J. (1999). Bone position estimation from skin marker co-ordinates using global optimisation with joint constraints. *J Biomech*, 32:129–134.

Lustig, S., Magnussen, R. A., Chèze, L., and Neyret, P. (2012). The kneekg system: a review of the literature. *Knee Surgery, Sports Traumatology, Arthroscopy*, 20(4):633–638.

Richard, V., Cappozzo, A., and Dumas, R. (2017). Comparative assessment of knee joint models used in multi-body kinematics optimisation for soft tissue artefact compensation. *J Biomech*. 62:95-101.

Richard, V., Lamberto, G., Lu, T., Cappozzo, A., and Dumas, R. (2016). Knee kinematics estimation using multi-body optimisation embedding a knee joint stiffness matrix: A feasibility study. *PLOS ONE*, 11(6):e0157010.

Scheys, L., Desloovere, K., Spaepen, A., Suetens, P., and Jonkers, I. (2011). Calculating gait kinematics using MR-based kinematic models. *Gait Posture*, 33(2):158–164.

Schneider, P. and Eberly, D. (2003). *Geometric Tools for Computer Graphics*. The Morgan Kaufmann Series in Computer Graphics and Geometric Modeling.

Shepherd, D. and Seedhom, B. (1999). Thickness of human articular cartilage in joints of the lower limb. *Ann Rheum Dis*, 58(1):27–34.

Söderkvist, I. and Wedin, P. (1993). Determining the movements of the skeleton using well-configured markers. *J Biomech*, 12:1473–1477.

Sreenivasa, M., Chamorro, C., Gonzalez-Alvarado, D., Rettig, O., and Wolf, S. (2016). Patient-specific bone geometry and segment inertia from MRI images for model-based analysis of pathological gait. *J Biomech*, 49(9):1918–1925.

Stagni, R., Fantozzi, S., and Cappello, A. (2009). Double calibration vs. global optimisation: Performance and effectiveness for clinical application. *Gait & Posture*, 29(1):119–122.

Stagni, R., Fantozzi, S., Cappello, A., and Leardini, A. (2005). Quantification of soft tissue artifact in motion analysis by combining 3D fluoroscopy and stereophotogrammetry: a study on two subjects. *Clin Biomech*, 20:320–329.

Tsai, T.-Y., Lu, T.-W., Kuo, M.-Y., and Lin, C.-C. (2011). Effects of soft tissue artifacts on the calculated kinematics and kinetics of the knee during stair-ascent. *J Biomech*, 44(6):1182–1188.

Valente, G., Pitto, L., Stagni, R., and Taddei, F. (2015). Effect of lower-limb joint models on subject-specific musculoskeletal models and simulations of daily motor activities. *J Biomech*, 48(16):4198–4205.

Walker, P., Rovick, J., and Robertson, D. (1988). The effects of knee brace hinge design and placement on joint mechanics. *J Biomech*, 21(11):965–974.

Wu, G., Siegler, S., Allard, P., Kirtley, C., Leardini, A., Rosenbaum, D., Whittle, M., D'Lima, D., Cristofolini, L., Witte, H., Schmid, O., and Strokes, I. (2002). ISB recommendation on definitions of joint coordinate system of various joints for the reporting of human joint motion - Part I: Ankle, hip and spine. *J Biomech*, 35(4):543–548.